

PREDICTION OF TWO-PHASE PIPE FLOWS USING SIMPLE CLOSURE RELATIONS IN A 2D TWO-FLUID MODEL

Svend Tollak Munkejord^{1*} Mona J. Mølsvik² Jens A. Melheim¹ Inge R. Gran²
 Robert Olsen¹

¹ Norwegian University of Science and Technology (NTNU),

Department of Energy and Process Engineering, Kolbjørn Hejes veg 1A, NO-7491 Trondheim, Norway

² SINTEF Energy Research, Energy Processes, Kolbjørn Hejes veg 1A, NO-7465 Trondheim, Norway

ABSTRACT

This paper presents a comparison of pressure drop and liquid hold-up as calculated using different modelling strategies; a two-dimensional two-fluid model, a one-dimensional simulator, and engineering correlations. The numerical results are compared with experimental data. Interestingly, the two-dimensional two-fluid model performed well, using simple constitutive relations being functions of the local flow conditions.

In the present work, a two-fluid model has been implemented in the framework of a two-dimensional multiphase Computational Fluid Dynamics (CFD) code. The governing equations were spatially discretized using the finite-volume technique, and the time-integrator was an explicit low-storage five-step fourth-order Runge-Kutta scheme.

Numerical results from the present program, the OLGAS simulator, the Beggs and Brill correlation, and the Friedel and the Premoli correlations have been compared to 52 data points from the TILDA two-phase pipe flow database at the SINTEF multiphase flow laboratory. The data were taken in a 0.189m inner-diameter pipe. The liquid volumetric flux j_ℓ varied between 0.1 and 1.0m/s, the gas volumetric flux j_g was in the range from 0.5 to 12m/s, and the pressure p ranged from 20 to 90bar. Inclination angles of 0 and 1° were used, with the majority of the data coming from the horizontal pipe.

We find it interesting to note the relatively good correspondence between experimental data and the computed results of the CFD program, particularly when considering the simple constitutive relations employed.

Keywords: multiphase flow, pipe flow, computational fluid dynamics (CFD), closure relations, pressure drop, liquid hold-up, explicit scheme

NOMENCLATURE

Latin letters

A	Area	m^2
\mathcal{A}	Control surface	m^2
B_k	Displacement factor	–
C	Friction parameter, see equation (14)	m^{-1}
C_μ, C_1, C_2	Constants in the k - ε turbulence model	–
c	Speed of sound	m/s
d	Diameter	m

E	Constant in wall function	–
F	Force per unit volume	N/m^3
f	Body force field	m/s^2
h	Channel height	m
I	Unitary tensor	–
j	Volumetric flux (superficial velocity)	m/s
k	Turbulence energy	m^2/s^2
N	Number of data points	–
δn	Normal distance from wall	m
n	Unit normal vector	m
P_k	Production rate of turbulence energy	m^2/s^3
p	Pressure	Pa
δp	Local pressure variation, see equation (6)	Pa
Re	Reynolds number	–
t	Time	s
$T_{k,w}$	Wall-function variable, see equation (29)	$Pa \cdot s/m$
u	Velocity vector	m/s
V	Volume	m^3
\mathcal{V}	Control volume	m^3
x	Length coordinate	m
y^+	Non-dimensional distance from wall in turbulent shear layer	–
y_0^+	Constant in wall function	–

Greek letters

α	Volume fraction	–
$\bar{\alpha}_\ell$	Liquid hold-up	–
ε	Dissipation rate of turbulence energy	m^2/s^3
Φ	Friction factor between phases k and l , see equation (13)	–
Γ	Mass source	$kg/(m^3s)$
κ	Constant in wall function	–
μ	Molecular viscosity	$Pa \cdot s$
μ^T	Eddy (turbulent) viscosity	$Pa \cdot s$
ρ	Density	kg/m^3
σ	Turbulent Prandtl/Schmidt number	–
τ_w	Wall shear stress	Pa
τ	Stress tensor	Pa
ψ	General variable	–

Subscripts

d	Drag	–
-----	------	---

*Corresponding author. E-mail: stm (a) pvv.ntnu.no

g	Gas	–
h	Homogeneous (no-slip)	–
i	Direction i in Cartesian coordinates	–
j	Direction j in Cartesian coordinates	–
k	Pertaining to phase k	–
l	Pertaining to phase l	–
ℓ	Liquid	–
m	Mixture	–
P	Near-wall point, see equation (28)	–
par	Parallel to wall, see equation (28)	–
w	Wall	–

Superscripts

\circ	Reference	–
T	Turbulent	–

1 INTRODUCTION

1.1 Background

A major challenge faced by the oil and gas industry stems from the tendency towards fields on deeper water situated at greater distance from the shore. This increases the drive towards field developments based on sub-sea processing and multiphase flow transportation. The older two-phase flow installations have gone off plateau and many of them now produce significant amounts of water. Water introduces new challenges related to flow assurance, exemplified by gas hydrates and scale deposits. Sub-sea processing, increased transport distance, and higher pipeline inclination in hilly terrain require qualified multiphase flow simulation tools.

Currently, one-dimensional simulation tools are routinely employed by engineers for designing and operating multiphase flow of oil and gas in long pipelines. OLGA is a dynamic modified two-fluid model developed primarily to simulate slow transients in two- and three-phase pipeline flow. The first version of OLGA was developed in 1979 and the model has been further developed by the Institute for Energy Technology (IFE) and Scandpower since then. The model uses two momentum equations, one representing the gas and possible liquid droplets and one representing the remaining liquid flow. The equations are solved numerically by a semi-implicit time-marching scheme.

One-dimensional models such as OLGA have enjoyed considerable success in predicting the intrinsically one-dimensional situation encountered in long pipelines. However, the above-mentioned problems exhibit two- and three-dimensional flows, e.g. in short pipes, bends and junctions, that are not suitable for one-dimensional approaches.

In the present work, a two-fluid model has been implemented in the framework of a two-dimensional multiphase Computational Fluid Dynamics (CFD) code. It differs from most other CFD simulators in that an explicit Runge-Kutta scheme is employed for advancing the solution in time. The presented results show that the multiphase equations are solved robustly and accurately. The method is suitable for efficient execution on massively parallel computers.

In this paper, we study two-phase high-pressure pipe flow. This is an important case since benchmark experimental data exist and because the performance of the simulator can be compared directly with dedicated pipeline models. Nevertheless, the motivation for the development of

a CFD simulator is to predict the flow in multidimensional geometries, such as valves, bends, separators, etc.

1.2 Previous work

Early numerical models of multiphase flows were most often tailored to a particular geometry, and specific flow regimes. Examples of such models are OLGAS (Bendiksen *et al.*, 1991) and various ones used in the nuclear industry. Improved and specialized models continue to be presented. Liné and Lopez (1997) made a two-fluid model of wavy separated two-phase flow, in which the shape of the gas–liquid interface was assumed to be known a priori, and where the momentum transfer was calculated using wave theory. Another approach was used by Newton and Behnia (2001), who solved the steady axial (one-dimensional) momentum equation together with a low-Reynolds-number k - ε turbulence model. A bipolar grid conveniently fitted the geometry of the stratified flow.

The use of two and three-dimensional CFD for multiphase flows can facilitate the solution of flows in complex geometries, as well as flow phenomena which otherwise could not be calculated. Early two-fluid flow codes primarily originate from single-fluid flow codes based on the Implicit, Continuous-fluid, Eulerian (ICE) solution scheme developed by Harlow and Amsden (1971) or the Semi-Implicit Method for Pressure-Linked Equations (SIMPLE) by Patankar and Spalding (1972). Examples of early two-fluid solution schemes are variants of the Implicit MultiField method (IMF) (Amsden and Harlow, 1974, 1978; Rivard and Torrey, 1977), the Inter-Phase Slip-Algorithm (IPSA) (Pun *et al.*, 1979; Spalding, 1980), Gas And Liquid Analyzer (GALA) (Spalding, 1977), and TRAC (Liles and Reed, 1978). Such semi-implicit methods are in use in several commercial CFD codes.

Moura and Rezkallah (1993) studied the two-phase flow distribution in a T-junction, and reported good agreement between calculated results and experimental data for the phase separation. Alajbegović *et al.* (1999) calculated particle/liquid pipe flows, and the radial position of the particles, and the axial and fluctuating velocities, compared fairly well with experiments.

Saurel and LeMetayer (2001) developed a multiphase model for compressible flows with interfaces, shocks, detonation waves and cavitation. This shows the potential of CFD models to solve a range of different problems. Although commercially available CFD codes are able to successfully predict some multiphase flows (Brown, 2002), several difficult problems persist, including such topics as accuracy and convergence.

Little work concerning CFD calculations of pressure drop and liquid hold-up of multiphase flow in horizontal pipes has been published. However, since relevant high-pressure experimental data for such setups exist, this is an interesting benchmark case.

1.3 Outline of paper

In the following section, our mathematical model will be presented in detail. Next, the numerical solution method is briefly described. Then the setup of the channel flow case study is explained, and the results of the present model are compared to those of other models and to experimental data. Finally, conclusions are drawn.

2 MULTI-FLUID MODEL

The multi-fluid equations can be deduced from the basic equations of single-phase flow. Several approaches have been used, for instance temporal averaging, volume averaging, and ensemble averaging (see e.g. Ishii, 1975; Soo, 1989; Drew and Passman, 1999). It is also possible to derive the multi-fluid equations without averaging, but by introducing distributions, i.e., generalized functions (Kataoka, 1986). In the present work, the volume-averaging approach presented by Soo (1989, Chapter 2) and Soo (1990, Chapter 6) has been employed. The different deductions lead to equations having the same form. However, the form of the unclosed terms and the interpretation of the variables in the equations may differ.

2.1 Basic equations

The volume-averaged continuity equation is

$$\frac{\partial}{\partial t} \langle \rho_k \rangle + \nabla \cdot \langle \rho_k \mathbf{u}_k \rangle = -\frac{1}{V} \int_{\mathcal{A}_k} \rho_k (\mathbf{u}_k - \mathbf{u}_s) \cdot \mathbf{n}_k \, dA = \Gamma_k, \quad (1)$$

and the volume-averaged momentum equation may be written as

$$\begin{aligned} \frac{\partial}{\partial t} \langle \rho_k \mathbf{u}_k \rangle + \nabla \cdot \langle \rho_k \mathbf{u}_k \mathbf{u}_k \rangle &= -\nabla \langle p_k \rangle + \nabla \cdot \langle \boldsymbol{\tau}_k \rangle + \langle \rho_k \rangle \mathbf{f} \\ &+ \frac{1}{V} \int_{\mathcal{A}_k} (-p_k \mathbf{I} + \boldsymbol{\tau}_k) \cdot \mathbf{n}_k \, dA \\ &- \frac{1}{V} \int_{\mathcal{A}_k} \rho_k \mathbf{u}_k (\mathbf{u}_k - \mathbf{u}_s) \cdot \mathbf{n}_k \, dA. \end{aligned} \quad (2)$$

Herein subscript k refers to phase k ; hence Einstein's summation rule does not apply. Further, the volume average of a variable ψ is defined by

$$\langle \psi_k \rangle = \frac{1}{V} \int_{\mathcal{V}_k} \psi_k \, dV, \quad (3)$$

and the intrinsic volume average is

$${}^i \langle \psi_k \rangle = \frac{1}{V_k} \int_{\mathcal{V}_k} \psi_k \, dV. \quad (4)$$

That is, $\langle \psi_k \rangle$ is averaged over the whole control volume \mathcal{V} , whereas ${}^i \langle \psi_k \rangle$ is averaged only over the part of the control volume where phase k is present, \mathcal{V}_k .

The integrals in Equations (1) and (2) appear due to the averaging. The average of time derivatives is rewritten using the Reynolds transport theorem, whereas the average of divergence and gradient terms is rewritten using the Slattery averaging theorem (Slattery, 1967; Whitaker, 1969). The resulting transfer integrals describe phase interactions due to pressure, viscous stresses, and inertia forces.

In the present work, the energy equation has not been considered. Further, the experimental data used in the comparison were adiabatic. It has been assumed that no mass transfer between the phases takes place:

$$\Gamma_k = 0, \quad (5)$$

which implies that the integrand of the second transfer integral in Equation (2) is zero. However, it is straightforward to include other expressions for mass transfer in our numerical model.

The transfer integral due to pressure and viscous stresses needs to be modelled. However, the pressure p_k on the interface is generally unknown. It is therefore convenient to assume that it may be written as the sum of the mean pressure in the control volume, and a local variation:

$$p_k = {}^i \langle p_k \rangle + \delta p_k. \quad (6)$$

A similar splitting was made by Drew and Passman (1999, Section 11.3.2).

The following relation between the gradient of the volume fraction $\alpha_k = V_k/V$ and the surface integral of the unit normal vector can be found, using the Slattery averaging theorem:

$$\nabla \alpha_k = -\frac{1}{V} \int_{\mathcal{A}_k} \mathbf{n}_k \, dA. \quad (7)$$

Insert Equations (6) and (7) into the pressure-part of the transfer integral of Equation (2):

$$\frac{1}{V} \int_{\mathcal{A}_k} -p_k \mathbf{I} \cdot \mathbf{n}_k \, dA = {}^i \langle p_k \rangle \nabla \alpha_k - \frac{1}{V} \int_{\mathcal{A}_k} \delta p_k \mathbf{n}_k \, dA. \quad (8)$$

For the pressure-gradient term of Equation (2), we have:

$$-\nabla \langle p_k \rangle = -\alpha_k \nabla {}^i \langle p_k \rangle - {}^i \langle p_k \rangle \nabla \alpha_k, \quad (9)$$

and the ${}^i \langle p_k \rangle \nabla \alpha_k$ term from the pressure gradient term and from the transfer integral are seen to cancel. Therefore, the volume-averaged momentum equation without phase change may be written as

$$\begin{aligned} \frac{\partial}{\partial t} \langle \rho_k \mathbf{u}_k \rangle + \nabla \cdot \langle \rho_k \mathbf{u}_k \mathbf{u}_k \rangle &= -\alpha_k \nabla {}^i \langle p_k \rangle + \nabla \cdot \langle \boldsymbol{\tau}_k \rangle \\ &+ \langle \rho_k \rangle \mathbf{f} + \frac{1}{V} \int_{\mathcal{A}_k} (-\delta p_k \mathbf{I} + \boldsymbol{\tau}_k) \cdot \mathbf{n}_k \, dA. \end{aligned} \quad (10)$$

2.2 Equation of state

The following equation of state gave the relation between pressure and density:

$$p_k = c_k^2 (\rho_k - \rho_k^\circ), \quad (11)$$

where the speed of sound c_k and the 'reference density' ρ_k° were constants.

2.3 Interface forces

The integral in Equation (10) was modelled the following way:

$$\frac{1}{V} \int_{\mathcal{A}_k} (-\delta p_k \mathbf{I} + \boldsymbol{\tau}_k) \cdot \mathbf{n}_k \, dA = -(1 - B_k) {}^i \langle p_k \rangle \nabla \alpha_k + \mathbf{F}_d, \quad (12)$$

where B_k is a 'displacement factor' close to unity, which can be regarded as a simplified model for forces causing dispersion of the volume fraction profile, e.g. in intermittent flow. See Appendix A.

\mathbf{F}_d is the drag force per unit volume, for which the following model was assumed (see e.g. Moura and Rezkallah, 1993):

$$\mathbf{F}_d = \sum_{\forall l \neq k} \Phi^{kl} \|\mathbf{u}_l - \mathbf{u}_k\| (\mathbf{u}_l - \mathbf{u}_k), \quad (13)$$

where

$$\Phi^{kl} = C \rho_m \alpha_k \alpha_l, \quad k \neq l \quad \text{and} \quad [C] = \text{m}^{-1}, \quad (14)$$

and where

$$\|\mathbf{u}\|^2 \equiv \mathbf{u} \cdot \mathbf{u}. \quad (15)$$

Herein, ρ_m is the mixture density:

$$\rho_m = \sum_{\forall k} \langle \rho_k \rangle. \quad (16)$$

The drag force \mathbf{F}_d on phase k is due to the presence of phase l , and it may be observed that the drag force is proportional to the square of the relative velocity between the phases. Further, the factor Φ^{kl} is proportional to the mixture density and the area density (interfacial area per unit volume) between the phases, and it approaches zero when one of the volume fractions α vanishes. C is a model constant with dimension $1/L$, where the appropriate length scale depends upon the flow regime, among other things.

Due to surface tension and other effects, the pressure may in general differ between the phases. In the present work, however, the pressure was taken to be the same in all phases.

2.4 Turbulence model

In the present work, turbulence was modelled by introducing a spatial fluctuation in the velocity (see e.g. Nigmatulin, 1991, page 35):

$$\mathbf{u}_k = \tilde{\mathbf{u}}_k + \mathbf{u}_k'', \quad (17)$$

\mathbf{u}_k is the velocity of phase k at a point inside the control volume \mathcal{V} at time t , while $\tilde{\mathbf{u}}_k$ is its mean, and \mathbf{u}_k'' is its spatial fluctuation. The mean velocity is defined by:

$$\tilde{\mathbf{u}}_k \equiv \frac{\langle \rho_k \mathbf{u}_k \rangle}{\langle \rho_k \rangle}, \quad (18)$$

which is mass-weighted or Favre averaged. Hence, the volume average of the spatial fluctuation is zero:

$$\langle \rho_k \mathbf{u}_k'' \rangle = 0. \quad (19)$$

Volume averaging can only be applied to quantities per volume or area. Therefore, when for instance velocity is averaged, it is necessary to include the density:

$${}^i\langle \mathbf{u}_k \rangle = \frac{1}{\langle \rho_k \rangle V} \int_{\mathcal{V}_k} \rho_k \mathbf{u}_k dV = \frac{\langle \rho_k \mathbf{u}_k \rangle}{\langle \rho_k \rangle}. \quad (20)$$

It follows from Equation (18) and Equation (20) that $\tilde{\mathbf{u}}_k = {}^i\langle \mathbf{u}_k \rangle$ when the Favre averaging is based on volume averaging. Therefore, the rules for Favre averaging can be applied to the volume-averaged equations.

The resulting Favre-averaged continuity equation is, when Equation (5) has been taken into account:

$$\frac{\partial}{\partial t} \langle \rho_k \rangle + \nabla \cdot \langle \rho_k \rangle {}^i\langle \mathbf{u}_k \rangle = 0, \quad (21)$$

and for the momentum Equation (10) we obtain

$$\begin{aligned} & \frac{\partial}{\partial t} \langle \rho_k \rangle {}^i\langle \mathbf{u}_k \rangle + \nabla \cdot \langle \rho_k \rangle {}^i\langle \mathbf{u}_k \rangle {}^i\langle \mathbf{u}_k \rangle = -\alpha_k \nabla^i \langle p_k \rangle \\ & - (1 - B_k) {}^i\langle p_k \rangle \nabla \alpha_k + \nabla \cdot \left(\langle \boldsymbol{\tau}_k \rangle + \boldsymbol{\tau}_k^T \right) + \langle \rho_k \rangle \mathbf{f} + \mathbf{F}_d, \end{aligned} \quad (22)$$

after using Equation (12). Here, $\boldsymbol{\tau}_k^T$ is the fluctuating stress tensor:

$$\boldsymbol{\tau}_k^T = -\langle \rho_k \mathbf{u}_k'' \mathbf{u}_k'' \rangle, \quad (23)$$

Table 1: Constants in the standard k - ε model.

C_μ	C_1	C_2	σ_k	σ_ε
0.09	1.44	1.92	1.0	1.3

which in the present work was modelled by the Reynolds stress tensor.

In the present work, a two-equation turbulence model was used. The single-phase k - ε model (Launder and Spalding, 1974) was extended to multiphase flows by appropriately accounting for the volume fraction of the phases. The equation for the turbulence energy k was as follows, written in Cartesian tensor notation:

$$\begin{aligned} & \frac{\partial \langle \rho_k k \rangle}{\partial t} + \frac{\partial \langle \rho_k k \rangle {}^i\langle u_{k,j} \rangle}{\partial x_j} \\ & = \frac{\partial}{\partial x_j} \left[\left(\alpha_k \mu_k + \frac{\mu_k^T}{\sigma_k} \right) \frac{\partial {}^i\langle k \rangle}{\partial x_j} \right] + P_{kk} - \langle \rho_k \varepsilon_k \rangle \end{aligned} \quad (24)$$

and the equation for the dissipation rate ε of turbulence energy was:

$$\begin{aligned} & \frac{\partial \langle \rho_k \varepsilon_k \rangle}{\partial t} + \frac{\partial \langle \rho_k \varepsilon_k \rangle {}^i\langle u_{k,j} \rangle}{\partial x_j} \\ & = \frac{\partial}{\partial x_j} \left[\left(\alpha_k \mu_k + \frac{\mu_k^T}{\sigma_\varepsilon} \right) \frac{\partial {}^i\langle \varepsilon_k \rangle}{\partial x_j} \right] \\ & \quad + C_1 \frac{{}^i\langle \varepsilon_k \rangle}{{}^i\langle k \rangle} P_{kk} - C_2 \frac{{}^i\langle \varepsilon_k \rangle}{{}^i\langle k \rangle} \alpha_k \rho_k \varepsilon_k, \end{aligned} \quad (25)$$

where the production P_{kk} of turbulence energy is given by:

$$\begin{aligned} P_{kk} = & \left[\mu_k^T \left(\frac{\partial {}^i\langle u_{k,i} \rangle}{\partial x_j} + \frac{\partial {}^i\langle u_{k,j} \rangle}{\partial x_i} \right) \right. \\ & \left. - \frac{2}{3} \delta_{ij} \left(\mu_k^T \frac{\partial {}^i\langle u_{k,l} \rangle}{\partial x_l} + \langle \rho_k k \rangle \right) \right] \frac{\partial {}^i\langle u_{k,i} \rangle}{\partial x_j}. \end{aligned} \quad (26)$$

The model for the eddy viscosity was:

$$\mu_k^T = C_\mu \langle \rho_k \rangle \frac{{}^i\langle k \rangle^2}{{}^i\langle \varepsilon_k \rangle}. \quad (27)$$

The constants are equal to Launder and Spalding (1974)'s constants, given in Table 1. 'Multiphase effects' and buoyancy effects that might affect the production and dissipation of turbulence energy, have not been considered in the above equations. This is a simplification. Multiphase effects are, however, accounted for to the extent that when the velocity gradients change, so does the production term (26) of the turbulence energy transport Equation (24).

2.5 Wall boundary

For the wall boundaries, a standard wall function for smooth walls was used (see Schlichting, 1979, page 602). It was extended to multiphase flow by accounting for the volume fraction of the phases, but disregarding other possible multiphase effects.

The wall shear stress was represented by the following expression:

$$\boldsymbol{\tau}_{k,w} = -\alpha_k T_{k,w} \left({}^i\langle \mathbf{u}_k \rangle_{P,\text{par}} - \mathbf{u}_{\text{wall}} \right), \quad (28)$$

Table 2: The constants in the wall function.

κ	E	y_0^+
0.4187	9.0	11.63

where \mathbf{u}_{wall} is the velocity of the wall, zero in the present study, and ${}^1\mathbf{u}_k)_{P,\text{par}}$ is the velocity vector parallel to the wall. $T_{k,w}$ is given by the wall function:

$$T_{k,w} = \begin{cases} \mu_k / \delta n_P & y_{k,P}^+ \leq y_0^+, \\ (\dot{i}_{\langle \rho_k \rangle} \tau_{k,1})^{1/2} \kappa / \ln(E y_{k,P}^+) & y_{k,P}^+ > y_0^+, \end{cases} \quad (29)$$

where

$$\tau_{k,1} = C_\mu^{1/2} \dot{i}_{\langle \rho_k \rangle} \dot{i}_{k,P}, \quad (30)$$

and

$$y_{k,P}^+ = \frac{(\dot{i}_{\langle \rho_k \rangle} \tau_{k,1})^{1/2} \delta n_P}{\mu_k}. \quad (31)$$

In Equations (28)–(31), subscript P refers to the near-wall point in the computational domain. δn_P is the normal distance from point P to the wall. $\tau_{k,1}$ is the shear stress in the internal sub-layer and is assumed to be equal to $\tau_{k,w}$, and $y_{k,P}^+$ is a dimensionless wall coordinate. The wall function constant for smooth walls are given in Table 2.

2.6 Numerics

Here we will briefly describe the numerical solution method. The equations were discretized using the finite-volume method on a curvilinear non-orthogonal collocated grid. The simulation program could use the power-law as well as the second-order upwind discretisation scheme (Mellaen, 1992). In the present case, the differences between the two were small.

The result of the application of discrete approximations for the spatial terms is that the governing equations constitute a set of coupled ordinary differential equations (ODEs). The remaining derivatives are then discretized in time by time steps.

Families of low-storage, explicit Runge-Kutta schemes have been derived and successfully applied for integrating the compressible Navier-Stokes equations (Kennedy *et al.*, 2000; Williamson, 1980). In the present study, the temporal integration of the semi-discretized governing equations was performed using the five-step fourth-order scheme by Carpenter and Kennedy (1994).

It is the Courant-Friedrichs-Lewy (CFL) number that determines the maximum time-step length, and here, the following estimate was used:

$$\text{CFL} = (|u| + c) \frac{\Delta t}{\Delta x}, \quad (32)$$

where c is the speed of sound, Δt is the time-step length and Δx is the grid spacing in the relevant direction. All of the present computations were run with $\text{CFL} = 1$, and the solutions were verified to be independent of the time-step length.

To avoid ‘checkerboard oscillations’, a fourth-order artificial dissipation filter was applied to the continuity and momentum equations. It used the Rhie and Chow (1983)

Table 3: The range of experimental data employed in the present study.

Quantity	Range	Unit
Liquid volumetric flux, j_ℓ	0.1–1.0	m/s
Gas volumetric flux, j_g	0.5–12	m/s
Pressure, p	20–90	bar
Pipe inclination angle, ϕ	0–1	°

momentum interpolation approach as a starting point. See also for instance Ferziger and Perić (1999, Section 7.5.2). Instead of using a pressure-based filter, which is sufficient in incompressible flow, the present filter is based on $\alpha\rho$ for the continuity equation and $\alpha\rho u$ for the momentum equations.

The present numerical method has been tested and the solutions have been found to converge by grid refinement.

3 CASE STUDY: CHANNEL FLOW

3.1 Introduction

One of the main points of CFD is the calculation of flows in complex geometries. However, experimental data for such geometries are scarce. The objective of the present study has therefore been to compare CFD calculations with experimental data from full-scale tests with real conditions. This was regarded as an important step in the validation of the CFD code.

The calculated results were compared to data from the SINTEF two-phase pipe flow database TILDA, which is used in the oil and gas industry. The data were taken in a pipe with an inner diameter d_i of 0.189 m (8" pipe) with two-phase flow of naphtha and nitrogen. The range of experimental data employed in the present study is shown in Table 3. Most of the data were horizontal. The flow regime was reported to be outside the slug range. The data are for high pressures, where there is a strong gas-liquid interaction. Hence, the slip between the phases is low.

The CFD calculations were performed two-dimensionally, with the hydraulic diameter corresponding to the inner diameter of the pipe, that is, with a channel height of $h = 1/2d_i$. Idelchik (1994) reports that for turbulent flow in a two-dimensional channel should be expected to be 10% higher than that of a channel with a square cross-section. However, for calculations of single-phase flow, this could neither be confirmed using the present computer program, nor with the commercial code Fluent 6.0. Therefore, in the present work, the calculated pressure drops were directly compared to the experimental data.

The experimental test loop was modelled as a 200 m long straight channel. With such a length, the flow was fully developed at the outlet. At the inlet, gas and liquid mass fluxes were specified, and plug velocity profiles were assumed. At the outlet, pressure was specified. Further, the liquid hold-up (mean liquid volume fraction) was calculated as

$$\bar{\alpha}_\ell = \frac{1}{h} \int_0^h \alpha_\ell dy, \quad (33)$$

while the gas and liquid volumetric fluxes (also referred to as ‘superficial velocities’ in the literature) were calculated

Table 4: Model parameters in the interface force models.

Quantity	Value	Unit
Displacement factor, B_k	0.99992	-
Friction parameter, C	30	m^{-1}

as

$$j_k = \frac{1}{h} \int_0^h \alpha_k u_k dy. \quad (34)$$

The inlet gas and liquid mass fluxes were varied in such a way that the outlet gas and liquid volumetric fluxes coincided with the values used in the experiments. Thus the calculated pressure gradient and liquid hold-up at the outlet could be compared to the experimental values.

For the present calculations, an orthogonal, Cartesian equidistant computational grid of 22 points (20 control volumes) in each coordinate direction was used. Typically, when the number of control volumes was doubled, the predicted pressure gradient and liquid hold-up changed in the order of 1%. This was considered to be less than the experimental uncertainty, and also less than the uncertainty in the currently employed constitutive relations.

It was necessary to assume values for the model parameters introduced in the interface force models. The displacement factor B_k (see Equation (12)) affects the volume fraction profiles. For all the calculations, it was set equal to $B_k = 0.99992$, see Table 4, which gave a relatively smooth transition between the liquid-dominated and the gas-dominated zones. To satisfy Newton's third law, B_k was set equal in both phases. The interface friction parameter C (see Equation (14)) was assigned a value of $C = 30 \text{m}^{-1}$. This implied a length scale in the order of centimetres, which seemed reasonable in the present case.

C and B_k were kept constant in all the calculations, i.e., different flow regimes were not explicitly accounted for. Importantly, no attempt was made to fit the calculated values to the experimental data by adjusting the parameters.

3.2 Calculated results and comparison with experimental data

In this section, the results obtained with the present program are compared with experimental data, and also with results from the 1D simulator OLGAS, and from engineering correlations.

In the present study, results from a total of $N = 52$ data points were evaluated. In addition to comparing our calculations with experimental data, we compared them to results obtained by using the stationary oil and gas pipeline simulator OLGAS 2000 v. 2.00. It is an engineering tool being in use in the oil and gas industry. OLGAS 2000 calculates the two-phase flow one-dimensionally, and its models have been fit to experimental data. OLGAS is a stationary version of the OLGAS model (Bendiksen *et al.*, 1991).

Furthermore, our calculations were compared to two engineering correlations; the Beggs and Brill (1973) correlation as presented in Brill and Mukherjee (1999) (without the Payne *et al.* modifications), and a combination of the Friedel (1979) correlation for the frictional pressure drop and the Premoli *et al.* (1971) correlation for the volume fraction (to determine the gravitational pressure drop and the liquid hold-up). The former correlation was developed specifically for two-phase flow in oil and gas pipelines,

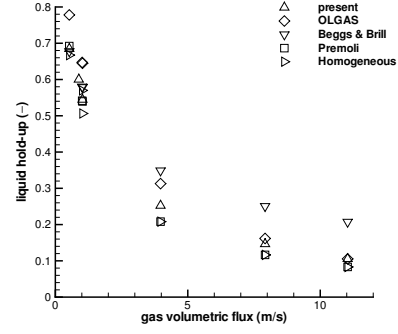


Figure 1: Calculated liquid hold-up $\overline{\alpha}_\ell$ as a function of gas volumetric flux j_g , for a pressure $p = 45$ bar and a liquid volumetric flux $j_\ell = 1$ m/s.

whereas the latter was made for air-water flow. These correlations are relatively well-known, and will not be repeated here.

3.2.1 Liquid hold-up vs. gas volumetric flux

Figure 1 shows liquid hold-up as a function of gas volumetric flux for a pressure of $p = 45$ bar and a liquid volumetric flux of $j_\ell = 1$ m/s in a horizontal pipe. The results from the present calculations are plotted together with data obtained with the OLGAS program, the Premoli correlation, and the Beggs and Brill correlation. The liquid hold-up calculated for homogeneous flow (equal gas and liquid velocities, or no-slip) is also shown in the figure. In the usual situation that the liquid does not flow faster than the gas, the liquid hold-up cannot attain lower values than those of homogeneous flow.

All the calculation methods captured the generally falling trend of the liquid hold-up $\overline{\alpha}_\ell$ for increasing gas volumetric fluxes j_g . The present program performed well, although with a slight underprediction for low j_g and a slight overprediction for high j_g . The Premoli correlation reproduced the experimental data well throughout, except, curiously, for $j_g = 4$ m/s. The OLGAS program predicted the liquid hold-up slightly too high for $j_g = 11$ m/s, but with an increasing overprediction for decreasing gas volumetric fluxes. The Beggs and Brill correlation performed oppositely, with a slight underprediction for low gas volumetric fluxes, but with a substantial overprediction for high ones.

A similar plot, but for a pressure of 20 bar and a liquid volumetric flux of 0.1 m/s, is given in Figure 2. For this case, the present model still predicts the high-gas-volumetric-flux data well, but it significantly underpredicts the liquid hold-up for low gas volumetric fluxes. The same can be said for the Premoli correlation, although with a slightly less pronounced underprediction for the low gas fluxes. The OLGAS program and the Beggs and Brill correlation performed similarly to what they did for the $p = 45$ bar, $j_\ell = 1$ m/s case.

3.2.2 Pressure drop vs. gas volumetric flux

Figure 3 compares calculated pressure drops $\frac{\partial p}{\partial x}$ for a pressure of $p = 45$ bar and a liquid volumetric flux of $j_\ell = 1$ m/s

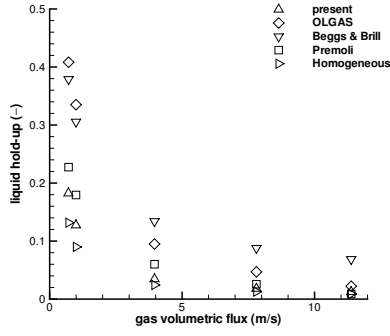


Figure 2: Calculated liquid hold-up $\bar{\alpha}_l$ as a function of gas volumetric flux j_g , for a pressure $p = 20$ bar and a liquid volumetric flux $j_l = 0.1$ m/s.

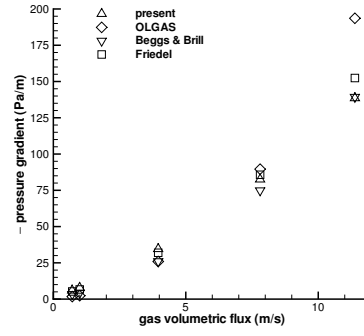


Figure 4: Calculated pressure drop $\frac{\partial p}{\partial x}$ as a function of gas volumetric flux j_g , for a pressure $p = 20$ bar and a liquid volumetric flux $j_l = 0.1$ m/s.

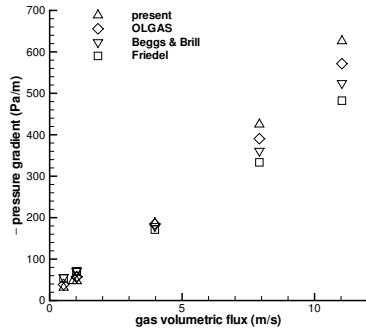


Figure 3: Calculated pressure drop $\frac{\partial p}{\partial x}$ as a function of gas volumetric flux j_g , for a pressure $p = 45$ bar and a liquid volumetric flux $j_l = 1$ m/s.

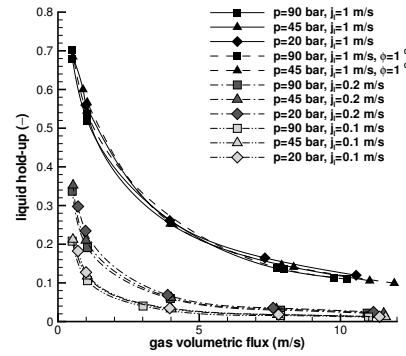


Figure 5: Computed liquid hold-up as a function of gas volumetric flux.

in a horizontal pipe. In this case, all calculation methods reproduced the experimental values reasonably well for the low gas volumetric fluxes. For increasing gas volumetric fluxes, the present program slightly overpredicted the pressure drop, whereas the OLGAS program slightly underpredicted it. This tendency of underprediction was more distinct for the Beggs and Brill correlation, and even more so for the Friedel correlation.

The case of a pressure of $p = 20$ bar and a liquid volumetric flux of $j_l = 0.1$ m/s is given in Figure 4. For the lowest gas volumetric fluxes j_g , the present program and the Friedel correlation overpredicted the pressure drop, whereas the OLGAS program and the Beggs and Brill correlation matched the experimental data quite well. For the highest gas volumetric flux, the present program and the Beggs and Brill correlation significantly underpredicted the pressure drop. The Friedel correlation underpredicted slightly less, while the pressure drop calculated by OLGAS only was a bit too high.

We hypothesize that the tendency of the present model increasingly to underpredict the pressure drop for increasing gas volumetric fluxes at low pressures and low liquid volumetric fluxes, may come as a result of different flow regimes not being explicitly accounted for. These are conditions where the slip factor is high, and the flow is expected to be inhomogeneous. Another contributing effect to the

underprediction may be the presently used wall function for smooth walls.

3.3 Liquid hold-up and pressure drop by the present program

Figure 5 shows liquid hold-up calculated by the present program as a function of gas volumetric flux, for varying pressure and liquid volumetric flux. Where the inclination angle ϕ is not indicated, the channel was horizontal. It can be observed that the liquid hold-ups fall on three lines; one for each liquid volumetric flux, virtually independent of pressure. (The curves have been fit to the calculated points to illustrate this.) Naturally, there is a falling tendency as the liquid volumetric flux decreases. Further, the liquid hold-up strongly increases when the gas volumetric flux is decreased.

Figure 6 gives the calculated pressure drop as a function of gas volumetric fluxes for different pressures and liquid volumetric fluxes. Line segments have been added between the calculated points to facilitate the reading of the figure. As expected, pressure drop increased with increasing gas and liquid volumetric fluxes. Further, it decreased for lower pressures, mainly due to a lower gas density.

The pressure drop was higher for the inclined channel ($\phi = 1^\circ$) because of the gravitational effect.

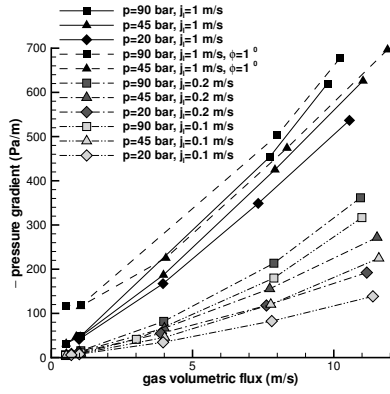


Figure 6: Computed pressure drop as a function of gas volumetric flux.

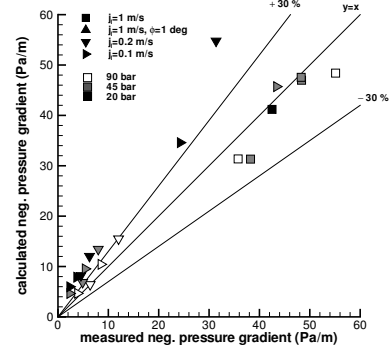


Figure 8: Comparison between experimental and computed pressure gradient (low-velocity data).

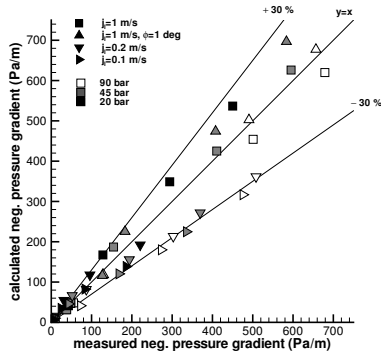


Figure 7: Comparison between experimental and computed pressure gradient.

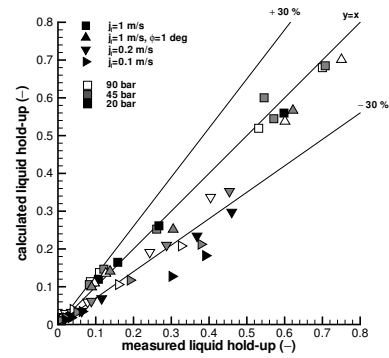


Figure 9: Comparison between experimental and computed liquid hold-up.

3.4 Comparison of all calculations to experimental data

An overview of the results of the present model for the pressure drop as compared to experimental data is given in Figure 7. All the evaluated data points can be seen in the graph. The measured values are plotted along the abscissa, and the calculated values are plotted along the ordinate. Therefore, ideally, all the points should fall on the line $y = x$. This is, however, not the case, due to the simplifications and uncertainties in the model, and to some extent also due to experimental uncertainty.

Figure 8 focuses on the low-velocity data. Figures 7–8 show that most of the data points fit between the $\pm 30\%$ lines. However, for the pressure drops below about 10 Pa/m (with liquid volumetric fluxes j_l below 0.2 m/s and gas volumetric fluxes below $j_g = 1 \text{ m/s}$), our model generally overpredicted the pressure drop. The pressure drop was more overpredicted for the lower pressures, where the density difference between gas and liquid was larger.

The data with a high liquid volumetric flux were represented fairly well by the present model. For the low liquid volumetric fluxes, the high-pressure-drop data (high gas volumetric fluxes) were mostly underpredicted, while there was a tendency to overpredict the low-pressure-drop data.

Figure 9 gives an overview for the results for the liquid hold-up, while Figure 10 focuses on low liquid hold-up.

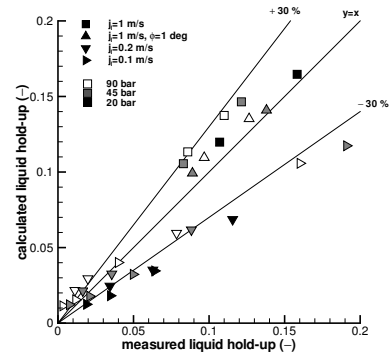


Figure 10: Comparison between experimental and computed liquid hold-up (low-liquid-hold-up data).

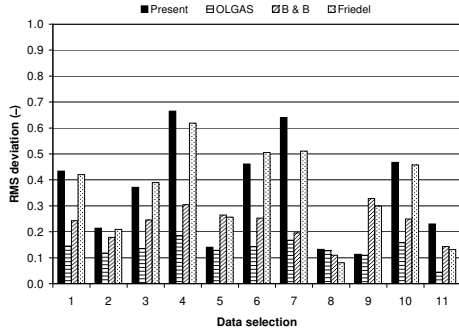


Figure 11: RMS deviations for pressure drop. The x-axis entries are explained in Table 5.

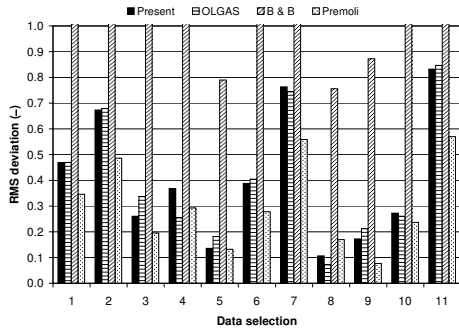


Figure 12: RMS deviations for liquid hold-up. The x-axis entries are explained in Table 5.

The calculated values compare reasonably well to the high-pressure and high-liquid-volumetric-flux data. However, there is a tendency towards underprediction for low pressures and low liquid volumetric fluxes.

3.5 Deviations between calculated values and experimental data

The discrepancies between calculated values and experimental data were evaluated by the root-mean-square deviation, defined by:

$$\sigma_{\text{rms}}(\psi) = \left[\frac{1}{N} \sum_{i=1}^N \left(\frac{\psi_{\text{calc},i} - \psi_{\text{exp},i}}{\psi_{\text{exp},i}} \right)^2 \right]^{\frac{1}{2}}. \quad (35)$$

The absolute deviation was also calculated, and gave the same trends.

The results for the pressure gradient and the liquid hold-up are shown in Table 5, and given graphically in Figures 11 and 12. The column labelled ‘ N ’ lists the number of data points. Note that a data point for, say, a pressure of $p = 90$ bar and a liquid volumetric flux of $j_\ell = 1$ m/s in a horizontal pipe will be counted in the categories 1, 2, 5, 9, and possibly 10 and 11. The table column labelled ‘F/P’ refers to the Friedel correlation for the pressure drop and the Premoli correlation for the liquid hold-up. The far-right column contains data where the calculations of the present program are compared with those of OLGAS instead of with the experimental data.

The categories 10 and 11 are somewhat special, and are further discussed in Section 3.5.3.

3.5.1 Pressure drop

All the tested calculation methods, except OLGAS, generally overpredicted the pressure drop. As can be observed, OLGAS had the smallest overall deviation (0.15), whereas the Beggs and Brill overall deviation was 0.24. This is not surprising, as those methods have been specifically tuned to match the pressure drop. The present CFD program and the Friedel correlation showed similar overall results, with overall deviations of 0.43 and 0.42, respectively.

OLGAS had the smallest deviations for all the data ranges, except for the inclined pipe (Case 8). (Case 9 consists of the corresponding data points for a horizontal pipe.) In Case 11, i.e., for high gas volumetric fluxes, the OLGAS predictions were very close to the experimental data. For the inclined pipe, the Friedel correlation performed best. The present model predicted the pressure drop more successfully for the highest liquid volumetric fluxes ($j_\ell = 1$ m/s).

It should be noted that in OLGAS, a pipe roughness of $2.9 \cdot 10^{-5}$ m was employed. For the present program and the two engineering correlations, the roughness was set to zero, as that gave better correspondence to the experimental data for the pressure drop.

3.5.2 Liquid hold-up

As for the liquid hold-up, the deviations given in Table 5, and illustrated by Figure 12, show that the best prediction was given by the Premoli correlation, with an overall RMS deviation of 0.35. It had a slight trend towards underprediction. The present model gave a deviation of 0.47, and the OLGAS code had virtually the same result.

It is interesting to note that the Premoli correlation gave the best results for the liquid hold-up for the studied data points, and that the present CFD program performed well, even though neither of these two models were developed specifically for oil and gas pipelines. The present program gave an overall deviation equal to that of OLGAS. The liquid hold-up predictions of the Beggs and Brill correlation gave an overall deviation one decade higher than those of the other models (3.6). (Note that as a result of this, in Figure 12, the bars representing the Beggs and Brill correlation significantly exceed the y axis scale for most of the cases). This was due to the Beggs and Brill correlation’s failing to predict the liquid hold-up for some of the data points with high gas volumetric fluxes j_g , particularly for high pressures. Moreover, even when these data points were disregarded, the Beggs and Brill correlation showed the largest deviations.

The Premoli correlation gave the smallest deviations for all the cases studied, except for the inclined pipe case (Case 8), where OLGAS was best, and Case 5 ($j_\ell = 1$ m/s), where the present program performed equally well. The present program performed relatively well for the highest liquid volumetric fluxes and for medium and high pressures.

3.5.3 Liquid hold-up for large Reynolds numbers

This section provides a discussion of the categories 10 and 11 in Table 5.

In category 10, the data points have been discarded where the measured liquid hold-up $\bar{\alpha}_{\ell,\text{exp}}$ was smaller than the liquid hold-up for homogeneous flow, $\bar{\alpha}_{\ell,\text{h}}$. Here, the term ‘homogeneous flow’ denotes a flow where the mean velocities of gas and liquid are equal, so that the liquid hold-up

Table 5: RMS deviations from experimental data.

Qty.	Range [*]	N	Present	OLGAS	B & B	F/P	Present [†]
$-\frac{\partial p}{\partial x}$	(1) All	52	0.434	0.145	0.243	0.420	0.676
	(2) $p = 90$ bar	18	0.214	0.117	0.179	0.209	0.315
	(3) $p = 45$ bar	20	0.372	0.135	0.245	0.390	0.522
	(4) $p = 20$ bar	14	0.665	0.184	0.304	0.619	1.087
	(5) $j_\ell = 1$ m/s	22	0.141	0.129	0.265	0.256	0.137
	(6) $j_\ell = 0.2$ m/s	15	0.461	0.142	0.253	0.505	0.667
	(7) $j_\ell = 0.1$ m/s	15	0.641	0.168	0.196	0.511	1.055
	(8) $\phi = 1^\circ$	8	0.132	0.127	0.109	0.080	0.113
	$j_\ell = 1$ m/s, $\phi = 1^\circ$						
	(9) $p = 90/45$ bar, $j_\ell = 1$ m/s, $\phi = 0^\circ$	8	0.113	0.110	0.328	0.299	0.132
	(10) $\overline{\alpha}_{\ell, \text{exp}} > \overline{\alpha}_{\ell, \text{h}}$	42	0.467	0.158	0.249	0.458	0.743
(11) $Re_g > 10^7$	12	0.230	0.044	0.143	0.131	0.216	
$\overline{\alpha}_\ell$	(1) All	52	0.468	0.470	3.614	0.346	0.336
	(2) $p = 90$ bar	18	0.673	0.679	5.540	0.486	0.241
	(3) $p = 45$ bar	20	0.261	0.337	2.362	0.196	0.306
	(4) $p = 20$ bar	14	0.368	0.254	1.049	0.293	0.460
	(5) $j_\ell = 1$ m/s	22	0.136	0.181	0.790	0.132	0.119
	(6) $j_\ell = 0.2$ m/s	15	0.388	0.404	2.564	0.278	0.392
	(7) $j_\ell = 0.1$ m/s	15	0.763	0.744	6.148	0.558	0.467
	(8) $p = 90/45$ bar, $j_\ell = 1$ m/s, $\phi = 1^\circ$	8	0.107	0.072	0.756	0.170	0.100
	(9) $p = 90/45$ bar, $j_\ell = 1$ m/s, $\phi = 1^\circ$	8	0.172	0.212	0.873	0.077	0.109
	(10) $\overline{\alpha}_{\ell, \text{exp}} > \overline{\alpha}_{\ell, \text{h}}$ $j_\ell = 1$ m/s, $\phi = 0^\circ$	42	0.272	0.261	1.074	0.237	0.372
	(11) $Re_g > 10^7$	12	0.832	0.847	7.273	0.570	0.079

^{*} Every data point matching the condition(s) listed, is counted in each range.

[†] The data in this column is for the present program with OLGAS, and *not* the experimental data, as reference.

could be calculated according to the formula

$$\overline{\alpha}_{\ell, \text{h}} = \frac{j_\ell}{j_g + j_\ell}. \quad (36)$$

A liquid hold-up smaller than that of homogeneous flow would imply that the mean liquid velocity was larger than the mean gas velocity. In the cases studied here, we consider such a behaviour unphysical. This shows that although the experiments have been conducted very carefully, experimental uncertainties will be present due to the demanding nature of these measurements.

Category 11 includes the data points where the gas Reynolds number $Re_g > 10^7$. It is defined by

$$Re_g = \frac{\rho_g j_g d}{\mu_g}. \quad (37)$$

Consider Figure 13. It shows the absolute relative deviation (i.e., $N = 1$ in Equation (35)) between liquid hold-up $\overline{\alpha}_\ell$ calculated by the present program and experimental data, as a function of gas Reynolds number Re_g . It can be seen that for low Reynolds numbers, the deviation has a mostly falling trend as the Reynolds number increases. However, at a Reynolds number of about $Re_g \approx 10^7$, the deviations start to increase, and for some of the data points very much so. Figure 14 shows a similar plot to that of Figure 13, but here, the reference is the OLGAS calculations. For low Reynolds numbers, the deviations are relatively high, and higher than those of Figure 13. Hence, the liquid hold-up calculated by the present program is closer to the experimental data than to the OLGAS calculations in that range. However, as the gas Reynolds number increases, the deviations decrease, and as opposed to the experimental data-based deviations, they continue to be low for the highest Reynolds numbers.

This effect is illustrated by Case 11 ($Re_g > 10^7$) in Table 5. All the calculation methods gave high deviations

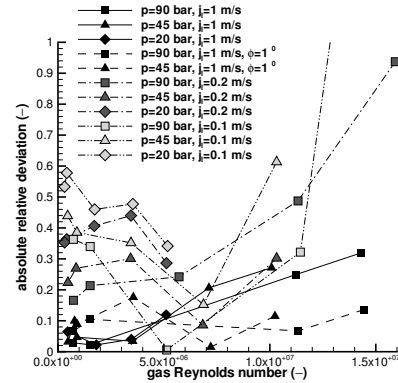


Figure 13: Absolute relative deviation between liquid hold-up calculated by the present program and experimental data, as a function of gas Reynolds number.

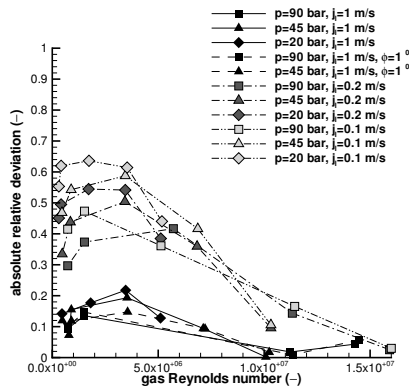


Figure 14: Absolute relative deviation between liquid hold-up calculated by the present program and by OLGAS, as a function of gas Reynolds number.

in this case. This is owing to the fact that all the data points¹ with a measured liquid hold-up smaller than the homogeneous-flow liquid hold-up fit into this category. It can be observed that the RMS deviations for the calculations of the present program and for those of OLGAS are nearly equal, with a value of 0.83 and 0.85, respectively, whereas the RMS deviation between the calculated results of the present program and those of OLGAS (last column in Table 5) is significantly smaller, with a value of 0.08. This shows that neither calculation method captured the measured data in this case. A further illustration can be given by comparing the Cases 1 and 10: All calculation methods have a significantly smaller deviation from the experimental data when the $\overline{\alpha}_{l,exp} < \overline{\alpha}_{l,h}$ data points are not considered.

4 CONCLUSIONS

We have presented a comparison of pressure drop and liquid hold-up calculated using different modelling strategies; a two-dimensional two-fluid model, a one-dimensional simulator, and engineering correlations. The numerical results have been compared with experimental data.

In the present work, a two-fluid model has been implemented in the framework of a two-dimensional multiphase Computational Fluid Dynamics (CFD) code. The governing equations were spatially discretized using the finite-volume technique, and the time-integrator was an explicit low-storage five-step fourth-order Runge-Kutta scheme.

Although the main purpose of a multiphase CFD model is to facilitate the design of process equipment, an important step in its validation is the comparison with good experimental data in simple geometries. The test case of high-pressure two-phase flow in pipes has been selected since it is of importance to the oil and gas industry.

Numerical results from the present program, the OLGAS simulator, the Beggs and Brill correlation, and the Friedel and the Premoli correlations have been compared to 52 data points from the TILDA two-phase pipe flow database. The data were taken in a 0.189 m inner-diameter pipe. The liquid volumetric flux j_l varied between 0.1 and 1.0 m/s, the gas volumetric flux j_g was in the range from 0.5 to 12 m/s, and pressures p from 20 to 90 bar were employed. Inclination

¹Except one

angles of 0 and 1° were used, with the majority of the data coming from the horizontal pipe.

The present program performed well at the higher pressures and at high liquid volumetric fluxes.

The liquid hold-up was slightly overpredicted for high gas volumetric fluxes and slightly underpredicted for low volumetric gas fluxes. For low pressures, the underprediction at low volumetric fluxes was significant.

At high pressure and high liquid volumetric fluxes, the calculated pressure drop compared well to the experimental data.

For low pressures and low liquid volumetric fluxes, the pressure drop was increasingly underpredicted for increasing gas volumetric fluxes. These are conditions where the slip factor is high, and the flow is expected to be inhomogeneous, so the underpredicted pressure drop may in part be due to different flow regimes not being explicitly accounted for.

The deviations between experimental data and model predictions are given in Table 5 on the preceding page. For the liquid hold-up, the predictions of the Friedel correlation had the lowest overall deviation. Interestingly, the present program had the same overall deviation as that of OLGAS. The Beggs and Brill correlation was not successful in predicting the liquid hold-up.

The smallest deviations between experimental and calculated pressure drops were obtained by the OLGAS program and the Beggs and Brill correlation. This is unsurprising, since the parameters in these models have been tuned to match experimentally observed pressure drops. The present program performed equally to OLGAS for high pressures and high liquid volumetric fluxes.

In some of the data points, the measured liquid hold-up was lower than that of homogeneous flow, and might be erroneous. The overall deviation for the liquid hold-up was significantly reduced for all the calculation methods when these data points were disregarded.

We find it interesting to note the relatively good correspondence between experimental data and the computed results of the CFD program, particularly when considering the simple constitutive relations employed.

ACKNOWLEDGEMENTS

The authors especially thank Kjell Arne Jacobsen of SINTEF Petroleum Research for providing data from the TILDA database. We would like to express our gratitude to Lars Hovden of Scandpower AS for performing the OLGAS calculations. We would also like to thank Professor Morten Chr. Melaaen at the Process Equipment Research Group at Telemark University College for his co-operation and useful suggestions for this article.

This work has been sponsored by the Research Council of Norway and by SINTEF Energy Research.

REFERENCES

- Alajbegović, A., Drew, D. A., and Lahey, R. T. An analysis of phase distribution and turbulence in dispersed particle/liquid flows. *Chemical Engineering Communications*, volume 174: pages 85–133, 1999.
- Amsden, A. A. and Harlow, F. H. KACHINA: An Eulerian computer program for multifield fluid flows. Technical

- Report LA-NUREG-5680, Los Alamos Scientific Laboratory, December 1974.
- Amsden, A. A. and Harlow, F. H. K-TIF: A two-fluid computer program for downcomer flow dynamics. Technical Report LA-NUREG-6994, Los Alamos Scientific Laboratory, January 1978.
- Beggs, H. D. and Brill, J. P. A study of two-phase flow in inclined pipes. *Journal of Petroleum Technology*, pages 607–617, May 1973.
- Bendiksen, K. H., Malnes, D., Moe, R., and Nuland, S. The dynamic two-fluid model OLGA: Theory and application. *SPE Production Engineering*, pages 171–179, May 1991.
- Brill, J. P. and Mukherjee, H. *Multiphase flow in wells*, volume 17 of *Henry L. Doherty series Monograph / SPE*, chapter Multiphase flow pressure gradient prediction. Henry L. Doherty Memorial Fund of AIME, Society of Petroleum Engineers, Richardson, Tex, USA, 1999.
- Brown, G. J. Erosion prediction in slurry pipeline tee-junctions. *Applied Mathematical Modelling*, volume 26, no. 2: pages 155–170, February 2002.
- Carpenter, M. H. and Kennedy, C. A. Fourth-order 2N-storage Runge-Kutta schemes. Technical Report TM 109111, NASA, April 1994.
- Drew, D. A. and Passman, S. L. *Theory of Multicomponent Fluids*. Number 135 in Applied Mathematical Sciences. Springer-Verlag, New York, 1999. ISBN 0-387-98380-5.
- Ferziger, J. H. and Perić, M. *Computational methods for fluid dynamics*. Springer-Verlag, Berlin, second edition, 1999. ISBN 3-540-65373-2.
- Friedel, L. Improved friction pressure drop correlations for horizontal and vertical two phase pipe flow. In: *Proceedings, European Two Phase Flow Group Meeting*. Ispra, Italy, June 1979. Paper E2.
- Harlow, F. H. and Amsden, A. A. Numerical fluid dynamics calculation method for all flow speeds. *Journal of Computational Physics*, volume 8, no. 2: page 197, 1971.
- Idelchik, I. E. *Handbook of hydraulic resistance*, chapter 2.2 Diagrams of friction coefficients. CRC Press, Boca Raton, Florida, USA, third edition, 1994. ISBN 0-8493-9908-4.
- Ishii, M. *Thermo-fluid dynamic theory of two-phase flow*. Collection de la Direction des Etudes et Recherches d'Electricité de France. Eyrolles, Paris, 1975.
- Kataoka, I. Local instant formulation of two-phase flow. *International Journal of Multiphase Flow*, volume 12, no. 5: pages 745–758, 1986.
- Kennedy, C. A., Carpenter, M. H., and Lewis, R. M. Low-storage, explicit Runge-Kutta schemes for the compressible Navier-Stokes equations. *Applied Numerical Mathematics*, volume 35, no. 3: pages 177–219, November 2000.
- Launder, B. E. and Spalding, D. B. The numerical computation of turbulent flows. *Computer Methods in Applied Mechanics and Engineering*, volume 3: pages 269–289, 1974.
- Liles, D. R. and Reed, W. H. Semi-implicit method for two-phase fluid-dynamics. *Journal of Computational Physics*, volume 26, no. 3: pages 390–407, 1978.
- Liné, A. and Lopez, D. Two-fluid model of wavy separated two-phase flow. *International Journal of Multiphase Flow*, volume 23, no. 6: pages 1131–1146, 1997.
- Melaen, M. C. Calculation of fluid-flows with staggered and nonstaggered curvilinear nonorthogonal grids – The theory. *Numerical Heat Transfer Part B – Fundamentals*, volume 21, no. 1: pages 1–19, January–February 1992.
- Moura, L. F. M. and Rezkallah, K. S. Numerical study on the two-phase flow distribution in a T-junction. *International Journal for Numerical Methods in Fluids*, volume 17: pages 257–270, 1993.
- Newton, C. H. and Behnia, M. A numerical model of stratified wavy gas-liquid pipe flow. *Chemical Engineering Science*, volume 56, no. 24: pages 6851–6861, December 2001.
- Nigmatulin, R. I. *Dynamics of Multiphase Media*, volume 1. Hemisphere Publishing Corporation, New York, 1991. ISBN 0-89116-316-6.
- Patankar, S. V. and Spalding, D. B. Calculation procedure for heat, mass and momentum-transfer in 3-dimensional parabolic flows. *International Journal of Heat and Mass Transfer*, volume 15, no. 10: page 1797, 1972.
- Premoli, A., Francesco, D., and Prina, A. A dimensionless correlation for determining the density of two-phase mixtures. *La Termotecnica*, volume 25: pages 17–26, 1971. In Italian.
- Pun, W. M., Spalding, D. B., Rosten, H., and Svensson, H. Calculation of two-dimensional steady two-phase flows. In: *Two-Phase Momentum, Heat and Mass Transfer in Chemical, Process, and Energy Engineering Systems*, F. Durst, G. V. Tsiklauri, and N. H. Afgan, editors, volume 1 of *Thermal and Fluids Engineering*, pages 461–470. Hemisphere, Washington, USA, 1979. ISBN 0-89116-104-X.
- Rhie, C.-M. and Chow, W. L. Numerical study of the turbulent flow past an isolated airfoil with trailing edge separation. *AIAA Journal*, volume 21, no. 11: pages 1525–1532, November 1983.
- Rivard, W. C. and Torrey, M. D. K-FIX: A computer program for transient, two-dimensional, two-fluid flow. Technical Report LA-NUREG-6623, Los Alamos Scientific Laboratory, April 1977.
- Saurel, R. and LeMetayer, O. A multiphase model for compressible flows with interfaces, shocks, detonation waves and cavitation. *Journal of Fluid Mechanics*, volume 431: pages 239–271, March 2001.
- Schlichting, H. *Boundary-Layer Theory*. McGraw-Hill, New York, 7 edition, 1979.

Sha, W. T. and Soo, S. L. Brief communication: On the effect of $P\nabla\alpha$ term in multiphase mechanics. *International Journal of Multiphase Flow*, volume 5, no. 2: pages 153–158, April 1979.

Slattery, J. C. Flow of viscoelastic fluids through porous media. *AIChE Journal*, volume 13, no. 6: pages 1066–1071, November 1967.

Soo, S. L. *Particulates and continuum: Multiphase fluid dynamics*. Hemisphere, New York, 1989. ISBN 0-89116-918-0.

Soo, S. L. *Multiphase fluid dynamics*. Science Press, Beijing, 1990. ISBN 0-291-39781-6, 70-300-0102.

Spalding, D. B. The calculation of free-convection phenomena in gas-liquid mixtures. In: *Heat Transfer and Turbulent Buoyant Convection*, D. B. Spalding and N. Afgan, editors, volume 2 of *Thermal and Fluids Engineering*, pages 569–586. Hemisphere, Washington, USA, 1977. ISBN 0-07-059926-2.

Spalding, D. B. Numerical computation of multi-phase fluid flow and heat transfer. In: *Recent Advances in Numerical Methods in Fluids*, C. Taylor and K. Morgan, editors, volume 1, pages 139–168. Pineridge Press, Swansea, UK, 1980. ISBN 0-906674-07-7.

Whitaker, S. Advances in theory of fluid motion in porous media. *Industrial and Engineering Chemistry*, volume 61, no. 4: pages 14–28, December 1969.

Williamson, J. H. Low-storage Runge-Kutta schemes. *Journal of Computational Physics*, volume 35, no. 1: pages 48–56, 1980.

A THE RANGE OF THE DISPLACEMENT FACTOR

B_k

Sha and Soo (1979) and Soo (1990, pages 319–321) maintained that the displacement factor B_k can attain values in the range 0–1. It can, however, be shown that B_k will be close to unity. Consider Equation (12). By rearranging, and using Equation (7), we get:

$$B_k = 1 - \frac{\frac{1}{V} \int_{\mathcal{A}_k} (-\delta p_k \mathbf{I} + \boldsymbol{\tau}_k) \cdot \mathbf{n}_k dA - \mathbf{F}_d}{\frac{1}{V} \int_{\mathcal{A}_k} i(p_k) \mathbf{I} \cdot \mathbf{n}_k dA} \quad (38)$$

In the numerator on the right-hand side of Equation (38), the terms will tend to cancel. Further, each of them will be small compared to the denominator. Hence B_k will be close to unity.